Numerical Modelling of Nearshore Circulation

by

Bruce A. Ebersole[1] and Robert A. Dalrymple[2], M.ASCE

INTRODUCTION

Waves impinging on beaches induce mean flows, such as longshore and rip currents. This nearshore circulation is of fundamental importance in the study of the transport of nearshore contaminants as well as littoral materials. Analytic models of this nearshore flow (see, e.g. 4, 9, 11, 12) have been constrained to be linear (in the governing equations) and simplistic in the bottom topography. Only recently have numerical models been developed to examine more complex situations. Steady state, finite difference models (1, 14), as well as a finite element model (10), have been proposed. The numerical model, developed by Birkemeier and Dalrymple (1), allowed for time dependency. Yet, in all of these cases, the governing equations have not included the nonlinear convective accelerations or lateral mixing terms.

In this study, a nonlinear numerical model is presented based on a leapfrog finite difference scheme, which includes time dependency and eddy viscosity terms. Results are shown for a planar beach showing a comparison with the analytical longshore current models (with and without lateral mixing) of Longuet-Higgins (11, 12). The longshore current over a prismatic beach profile including an offshore bar is presented next, showing the effects of the bar on the velocity profile. The circulation set-up by a rip channel inset into a plane beach is then computed. A comparison is made to the linear model of Birkemeier and Dalrymple. Finally the model is applied to the case of synchronous intersecting wave trains (4). An interesting result occurs when the waves are of different amplitudes, which could provide an explanation of the formation of finger bars on a beach.

GOVERNING EQUATIONS

The numerical model is formulated using the usual time-averaged (over one wave period) and depth-averaged conservation equations of mass and momentum, written in terms of the mean horizontal velocities (U, V) and the mean free surface displacement $\bar{\eta}$. These are

$$\frac{\partial \bar{\eta}}{\partial t} + \frac{\partial}{\partial x}(UD) + \frac{\partial}{\partial y}(VD) = 0 \tag{1}$$

$$\frac{\partial}{\partial t}(UD) + \frac{\partial}{\partial x}(U^2D) + \frac{\partial}{\partial y}(UVD) = -gD\frac{\partial \bar{\eta}}{\partial x} - \frac{1}{\rho}\left[\tau_{b_x} + \frac{\partial S_{xx}}{\partial x} + \frac{\partial S_{xy}}{\partial y} + D\frac{\partial \tau_\ell}{\partial y}\right] \tag{2}$$

[1]U. S. Army Waterways Experiment Station, Vicksburg, MS.

[2]Associate Professor, Department of Civil Engineering, University of Delaware, Newark, DE.

$$\frac{\partial}{\partial t}(VD) + \frac{\partial}{\partial x}(UVD) + \frac{\partial}{\partial y}(V^2D) = -gD\frac{\partial \bar{\eta}}{\partial y} - \frac{1}{\rho}\left[\tau_{b_y} + \frac{\partial S_{xy}}{\partial x} + \frac{\partial S_{yy}}{\partial y} + D\frac{\partial \tau_\ell}{\partial x}\right] \quad (3)$$

where $D = h + \bar{\eta}$, the total depth, h is the local still water depth, τ_{b_x} and τ_{b_y} are the bottom frictions in the x and y directions, τ_ℓ is the lateral shear stress due to turbulent velocity fluctuations, and ρ is the water density. The radiation stress terms, introduced by Longuet-Higgins and Stewart (see 13, 15), are specified throughout the region of interest in terms of the local wave energy and direction, θ. This information is supplied independently using a coupled wave refraction procedure modified from Noda et al. (14), which includes wave-current interaction, and wave breaking (based on a breaking index model for wave heights within the surf zone).

The bottom shear stress in each direction is found by numerically integrating over a wave period the nonlinear stresses

$$\left.\begin{aligned} \tau_{b_x} &= \frac{1}{T}\int_0^T \frac{\rho f}{8}\left|\bar{U} + \bar{U}_w\right|(U + U_m \cos\theta \cos\sigma t)dt \\ \tau_{b_y} &= \frac{1}{T}\int_0^T \frac{\rho f}{8}\left|\bar{U} + \bar{U}_w\right|(V + U_m \sin\theta \cos\sigma t)dt \end{aligned}\right\} \quad (4)$$

where the vertical bars denote absolute value (to ensure that the shear stress acts counter to the total velocity vector $\bar{U} = (U, V)$) and $\bar{U}_w = (U_m \cos\theta\, \bar{i} + U_m \sin\theta\, \bar{j})\cos\sigma t$[1], which is the wave orbital velocity vector at the bottom. Through experimentation, 16 terms in a Simpson's rule integration yielded bottom stress results with sufficient accuracy.

FINITE DIFFERENCE FORMULATION AND SOLUTION TECHNIQUE

In order to use a finite difference technique, the region of interest must first be discretized into a grid system as shown in Figure 1, with x positive offshore and y in the longshore direction. All the variables of interest except the velocities are defined at the center of each grid (the centers being separated by distances of Δx and Δy in the x and y directions). The horizontal velocities, on the other hand, are defined at the grid boundaries and are positive if they enter a grid in the positive coordinate direction.

To numerically solve the governing equations, they were approximated by their finite differenced forms. Following the methods of Lilly (8) and Blumberg (3), certain differencing and averaging operators are defined:

$$\delta_x[F(x,y,t)] = \frac{1}{\Delta x}\left[F\left(x + \frac{\Delta x}{2}, y, t\right) - F\left(x - \frac{\Delta x}{2}, y, t\right)\right] \quad (5)$$

$$\delta_x\overline{[F(x,y,t)]}^x = \frac{1}{2\Delta x}[F(x + \Delta x, y, t) - F(x - \Delta x, y, t)] \quad (6)$$

[1] U_m given by linear wave theory.

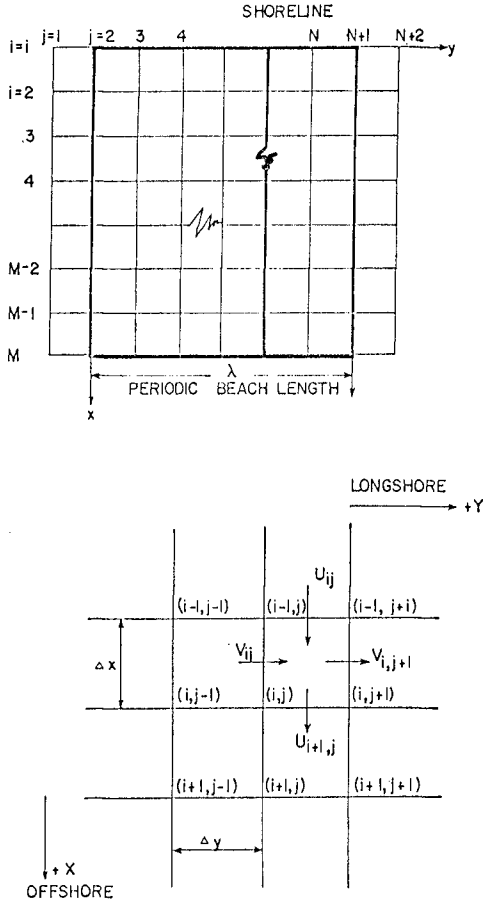

Figure 1. Discretization of Nearshore Region and Detail of Grid.

$$\overline{F(x,y,t)}^{x} \equiv \frac{1}{2}\left[F\left(x + \frac{\Delta x}{2}, y, t\right) + F\left(x - \frac{\Delta x}{2}, y, t\right)\right] \tag{7}$$

$$\overline{\overline{F(x,y,t)}^{x}}^{y} \equiv \overline{\overline{F(x,y,t)}^{y}}^{x} \tag{8}$$

The first two operators are essentially central finite differences about the point (x,y) over one spacial grid step, or two. Equations (7) and (8) are horizontal spacial averages in the x direction first then in both the x and y directions. Note that F(x,y,t) may be any function that varies in space and time and that similar operators exist for the variables y and t.

Using these operators the governing equations can be written in their differenced forms as,

CONTINUITY: $$\delta_t(\overline{\eta}^{t}) + \delta_x(\overline{D}^{x}U) + \delta_y(\overline{D}^{y}V) = 0 \tag{9}$$

x-MOMENTUM: $$\delta_t(\overline{\overline{D}^{x}U}^{t}) + \delta_x(\overline{\overline{D}^{x}U\,\overline{U}^{x}}^{x}) + \delta_y(\overline{\overline{D}^{y}V\,\overline{U}^{y}}^{x}) =$$

$$- g\overline{D}^{x}\delta_x(\eta) - \frac{1}{\rho}\left\{\overline{\tau_{b_x}}^{x} + \delta_y(\overline{S_{xy}}^{xy}) + \delta_x(S_{xx})\right\}$$

$$+ \overline{D}^{x}\delta_y[\varepsilon_y\delta_y(U)] + \overline{D}^{x}\delta_y[\overline{\varepsilon_x}^{xy}\delta_x(V)] \tag{10}$$

y-MOMENTUM: $$\delta_t(\overline{\overline{D}^{y}V}^{t}) + \delta_x(\overline{\overline{D}^{x}U\,\overline{V}^{y}}^{x}) + \delta_y(\overline{\overline{D}^{y}V\,\overline{V}^{y}}^{x}) =$$

$$- g\overline{D}^{y}\delta_y(\eta) - \frac{1}{\rho}\left\{\overline{\tau_{b_y}}^{y} + \delta_y(S_{yy}) + \delta_x(\overline{S_{xy}}^{xy})\right\}$$

$$+ \overline{D}^{y}\delta_x[\varepsilon_y\delta_y(U)] + \overline{D}^{y}\delta_x[\overline{\varepsilon_x}^{xy}\delta_x(V)] \tag{11}$$

In converting these differenced equations into the i, j notation of Figure 1 it is important to note that the x,y coordinate is defined at the location where the variable of interest, to be solved for in a particular equation, is defined. For example, the x-momentum equation is used to solve for the horizontal velocity, U, so the x,y coordinate is defined to be at the grid edge where $U_{i,j}$ is defined. Also in the above equations the bottom friction and lateral mixing terms were lagged one step in time to increase the computational stability, (3) and (6).

Before the problem can be solved numerically, initial and boundary conditions must be specified. In all applications of the model the initial conditions were assumed to be the state of rest. The mean

velocity and mean free surface displacement fields were set to zero, a still water depth matrix was specified, and the wave characteristics were determined using the procedures of Noda et al. The boundary conditions are as follows: at the first dry grid row and at the offshore grid row, M, no flow conditions were imposed by setting the velocity components equal to zero. This choice of boundary condition essentially simulates a wall at the onshore and offshore extremities of the area of interest. The onshore condition provides that there is no flow into the beach while the offshore condition is valid if, as the model approaches a steady state, the circulation due to longshore and offshore flows is negligible at row M-1. In the y-direction periodic boundary conditions were invoked. Referring again to Figure 1 periodicity requires that, for a quantity Q,

$$\left.\begin{aligned} Q(i,1) &= Q(i,N) \\ Q(i,2) &= Q(i,N+1) \\ Q(i,3) &= Q(i,N+2) \end{aligned}\right\} \qquad (12)$$

and so forth. Periodicity in the longshore direction was chosen because circulation patterns in nature are oftentimes periodic. Also if a particular stretch of beach, lacking periodicity, is being investigated, the boundaries in the model may be placed far enough away from this area of interest so that it does not affect the flow in this region, making the choice of periodic boundary conditions valid.

The differenced equations, (9) through (11), were derived using a central difference in time, for the time dependent terms, in which case they can be written as

$$\eta_{i,j}^{n+1} = \eta_{i,j}^{n-1} + 2\Delta t F_1^{n,n-1} \qquad (13)$$

$$U_{i,j}^{n+1} = AU_{i,j}^{n-1} + 2\Delta t F_2^{n,n-1} \qquad (14)$$

$$V_{i,j}^{n+1} = BV_{i,j}^{n-1} + 2\Delta t F_3^{n,n-1} \qquad (15)$$

where A and B are functions of depth alone, F_1, F_2 and F_3 are functions of all the variables in the problem, and n+1, n-1, and n denote time levels. These equations represent the leapfrog technique used to solve the problem in which updated values of η, U, and V are calculated using quantities defined at the previous two time levels. Everytime updated values of these three variables are computed, they are used to solve for the wave parameters at the same time level. In order to initiate the leapfrog scheme a forward difference in time using the initial conditions was implemented to establish variables defined at time levels 2 and 1. The leapfrog procedure was used for the duration of the computational steps. However, as the model approached a steady state, the solution diverged into two disjoint solutions, one following the even times steps and the other the odd. In order to correct this time-splitting problem, an Euler backward correction scheme (7) was used

every tenth iteration to "tie" the solutions back together. The following two equations describe the backward corrector,

$$h^* = h^{n-1} + 2\Delta t G \tag{16}$$

$$h^{n+1} = h^n + \Delta t G^* \tag{17}$$

Equation (16) is essentially any one of Equations (9) through (11) where "*" denotes the updated value of the variable of interest whether it be η, U or V. The function G is then computed using the new variable values and the new value at this time n+1, is computed. Equation (17) is a backward difference to the time step n from n+1. This correction scheme was chosen because it selectively damps the artificial computational mode of the solution, which can occur, while leaving the physical mode relatively unaffected. With the usage of this correction scheme the solution proceeded to reach a steady state with no further instability.

Due to the nonlinearities of the problem, an exact stability criterion for the choice of the time step, Δt, could not be established. Therefore, in applications of the model the time step was chosen to be significantly lower than the two-dimensional Courant stability criterion given by

$$\Delta t \leq \frac{\sqrt{(\Delta x)^2 + (\Delta y)^2}}{\sqrt{g h_{max}}}$$

RESULTS

Prismatic Beaches--The model was first applied to the case of a single progressive wave train approaching a planar beach (slope of 0.025) at some angle to the beach normal. The following input data was used. The deep water wave characteristics were: (1) a period of 8.0 seconds; (2) an angle of 30.0 degrees; and (3) a height of 2.0 meters built up over 200 (Δt = 0.5 second) iterations to avoid "shock" loading the system. The region of interest was broken into a 6 x 30 grid mesh with spacings of 10.0 and 15.0 meters in the x and y directions, respectively. The bottom friction factor, f, was chosen to be 0.08 and the mixing coefficients N and ϵ_y were chosen to be 0.01 and 0.5 meters^2/sec. The model was run for 1200 iterations which was nearly steady state.

The steady longshore current distributions both with and without mixing included are shown in Figure 2 along with the analytical results of Longuet-Higgins for the same input data. The major differences between the two profiles that exclude mixing are the sharpness of the discontinuity at the breaker line, and the difference in peak velocities. The numerical model shows less of a discontinuity in the breaker zone due to the fact that velocities just outside the surf zone are calculated using those from within the surf zone in the differenced form of the y-momentum equation, which results in a numerical "mixing". Also due to the use of a discrete grid size in the x-direction the exact location

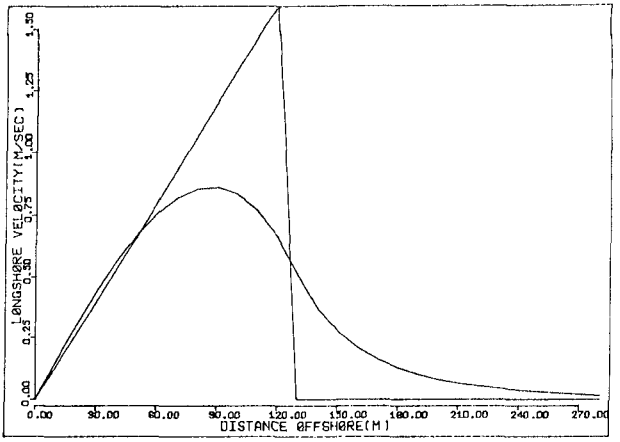

Figure 2a. Analytical Models of Longshore Current, With and Without Mixing [Longuet-Higgins (11, 12)].

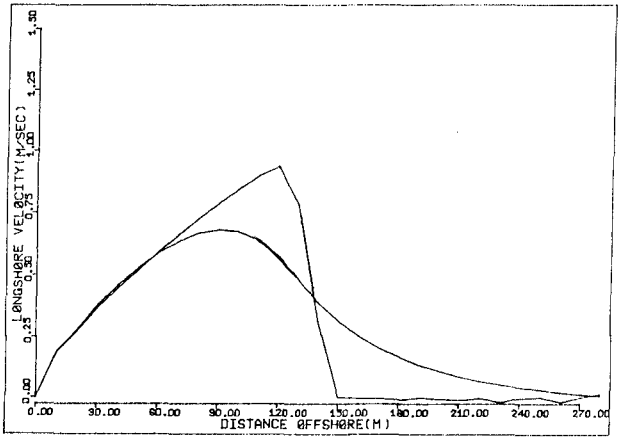

Figure 2b. Numerical Model Results for Longshore Current, With and Without Mixing.

of the breaker line is not adequately determined, resulting in a breaker line smoothing. As the grid size is decreased the location of the breaker line becomes better defined, making the discontinuity sharper as well as increasing the peak velocity. It must be noted that the peak velocities predicted by the model should not equal those resulting from Longuet-Higgins' theory due to the bottom friction formulation used in the model which was shown by Liu and Dalrymple (9) to decrease the analytical result by about 20% for the breaker angle and bottom slope found in this case.

In reality this strong discontinuity doesn't exist, and longshore current distributions tend to exhibit the properties shown by both the model and Longuet-Higgins results including mixing. These properties include: (1) a slight increase in velocities in the inner one-half of the surf zone; (2) a shift of the peak velocity from the breaker line shoreward; and (3) a slow decrease in the current to zero some distance beyond the breaker line.

Since in nature beach topographies often include longshore bars, the model was run on a bottom with an infinitely long longshore bar whose cross section is shown in Figure 3 in relation to a plane beach with slope 0.025. The remaining input into the model was identical to that used in the plane beach runs. The results for the model not including mixing are also shown in Figure 3. Notice the two distinct regions where a longshore current distribution exists. The velocity "spike" offshore is due to the waves breaking on the bar. As the wave height decreases, as a result of breaking, an onshore-offshore gradient of y-momentum flux is created which drives a longshore current. In the trough, however, the wave height starts to reform (no more breaking) resulting in the absence of a longshore current in this region. In reality a longshore current does exist in the trough, Allender et al. (1), due to the mechanisms of turbulent dissipation during breaking within a bore, lateral mixing which has been included in the model, and a set-up of water within the trough, Dalrymple (5). Figure 3b shows the velocity profile for the run including mixing. Note the reduction in current amplitude of the offshore "spike" and the smoothing of discontinuities resulting in the existence of a longshore current in the bar trough. Had the turbulent energy dissipation mechanism been included in the model the results would probably have approached those found in nature.

Periodic Bottom Topography Application--The model was next applied to the periodic bottom topography developed by Noda et al. (14) which is essentially a channel at some angle to the beach normal. The formulation for this bottom configuration is given in Appendix A. The model, including the effects of mixing, was compared to the linear model of Birkemeier and Dalrymple. The following wave characteristics were used in both instances: (1) deep water wave height of 1.0 meters; (2) wave period of 4.0 seconds; and (3) a deep water wave angle of 30.0 degrees to the beach normal. The bottom friction factor, f, was chosen to be 0.08, and the mixing coefficients, N and ε_y, were chosen to be 0.005 and 0.5 meters^2/sec., respectively. In both runs the wave height was built up to its deep water value over 100 seconds.

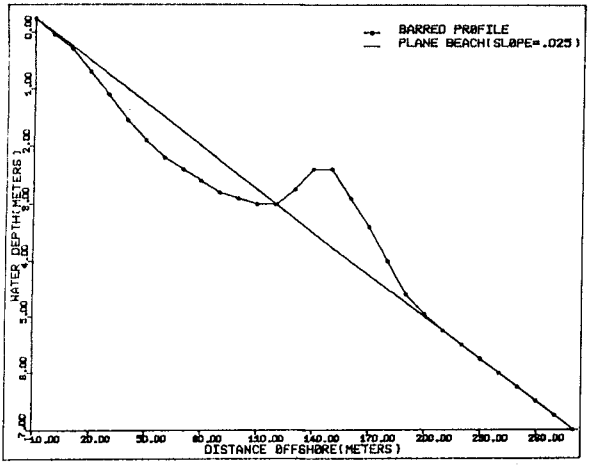

Figure 3a. Beach Profile for Planar and Barred Beach.

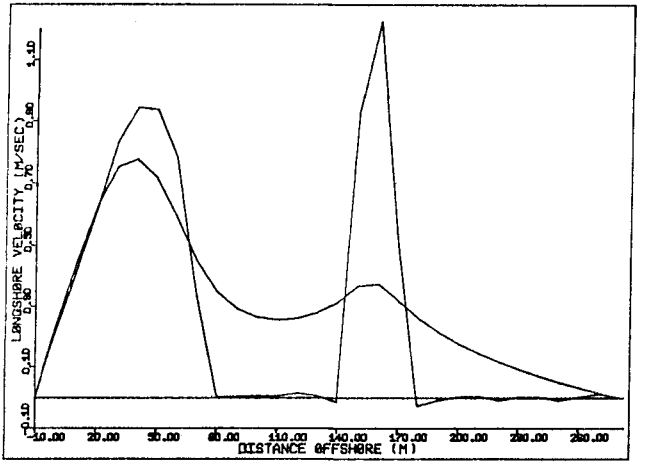

Figure 3b. Longshore Current Profiles on Barred Beaches, With and Without Mixing.

Both models were run until they reached approximately a steady state, about 500 seconds. The wave-current interaction process was halted in the linear model after 150 seconds because the offshore velocity components grew too large for the refraction routines to handle (i.e. wave breaking occurred in the rip channel). In the nonlinear model, however, the wave-current interaction process was included for the duration of the run time. The circulation patterns after 500 seconds are shown in Figure 4 and 5.

Note the strength of the rip and its offshore extent in the linear model compared to the nonlinear model. The peak velocity in the linear model run is about 3.0 meters per second whereas in the nonlinear model it is about 0.8 meters per second. This large discrepancy is due to the inclusion of mixing in the nonlinear model. The mixing tends to spread the rip out and decrease its offshore velocity components thus causing the rip to turn more in the longshore direction as shown in Figure 5. The effects of the convective acceleration terms are not clearly visible because it seems as though the form of the rip itself is governed primarily by horizontal mixing in this case. It is reasonable to expect, however, that in nature the lateral mixing in the rip current is far less than used here.

Synchronous Intersecting Waves--The final application of the model was to the case of intersecting wave trains of a common frequency on a plane beach which Dalrymple (4) showed could generate rip currents. The purpose here was to show the effect of the convective acceleration terms in the model. Certain changes were made to the model, namely: (1) the refraction routines of Noda et al. were replaced with those using Snells' law without wave-current interaction; (2) lateral mixing was excluded; (3) the "exact" bottom friction formulation was made to include two waves; (4) the radiation stresses due to both intersecting wave trains were calculated analytically for use in the momentum equations.

The waves were of equal heights (0.25 meters) and of equal deep water angles on either side of the beach normal (30.0 degrees). The period was chosen to be 7.1594 seconds which resulted in periodic rip currents with a spacing of 80.0 meters. The plane beach (slope 0.025) was broken into a planform area of 25 grids in the x-direction with a Δx spacing of 5.0 meters, and 21 grids in the y-direction with a Δy spacing of 4.0 meters. The time step was chosen to be 0.2 seconds and the wave was built up for 500 of the 1500 iterations run. The friction factor, f, was selected as 0.12 to allow the system to reach steady state faster and to decrease the magnitude of the resultant currents.

The total free surface described by these two wave trains is in essence a normally incident wave with a periodically modulated height. This is the driving mechanism which produces the rip currents shown in Figure 6. Note the constricted width of the rip current in relation to the width of the inflow region. This is a result of the convective acceleration terms. Also note the weak rip head where the currents diverge from the rip axis and return towards shore.

When one wave is of greater height than the other, all other variables remain the same, then a longshore current is superimposed over the cellular circulation, Figure 7.

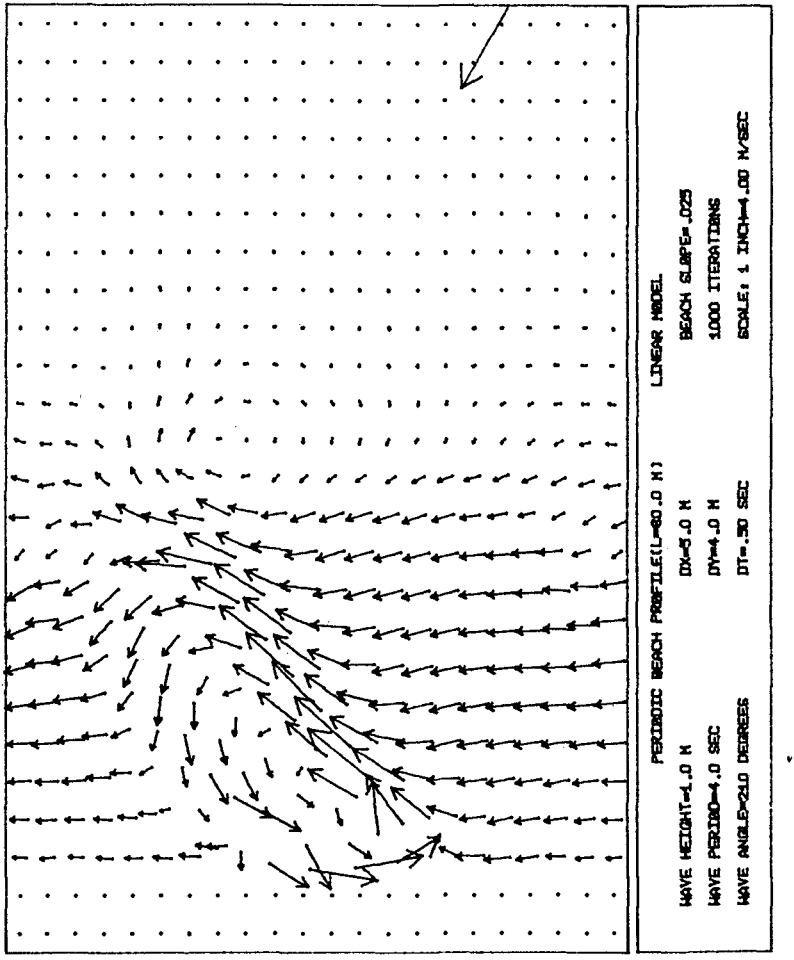

Figure 4. Current Vector Plot for the Model of Birkemeier and Dalrymple Run on the Periodic Bottom Topography.

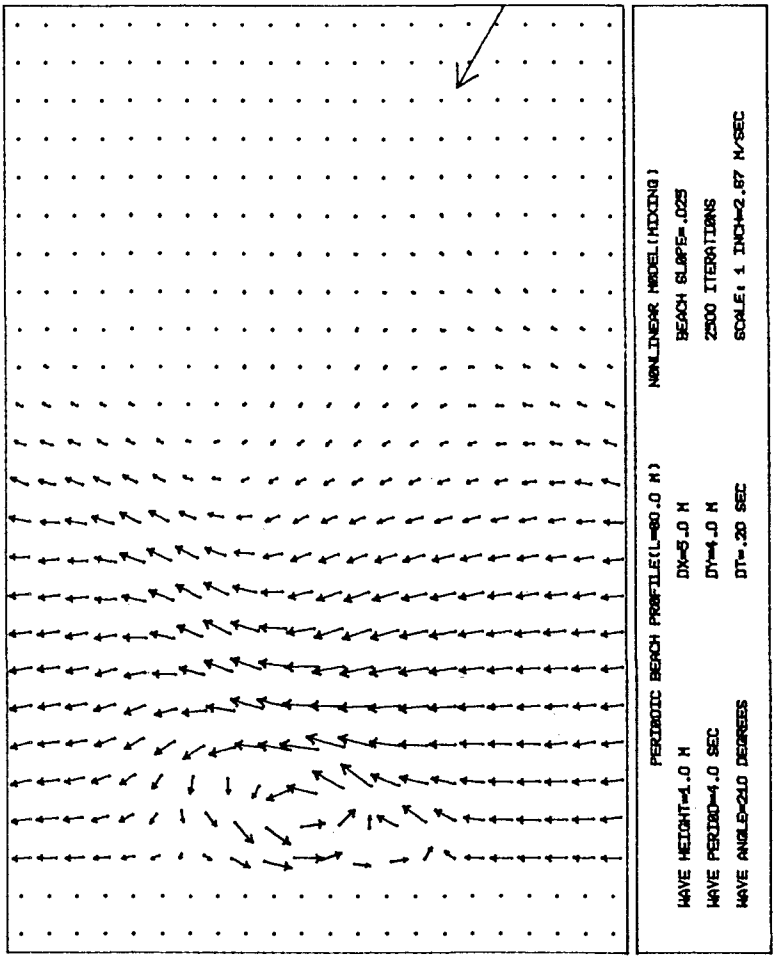

Figure 5. Current Vector Plot for the Present Model Including Mixing Run on the Periodic Bottom Topography. The Arbitrary Longshore Mixing Coefficient Probably Chosen as Too Large.

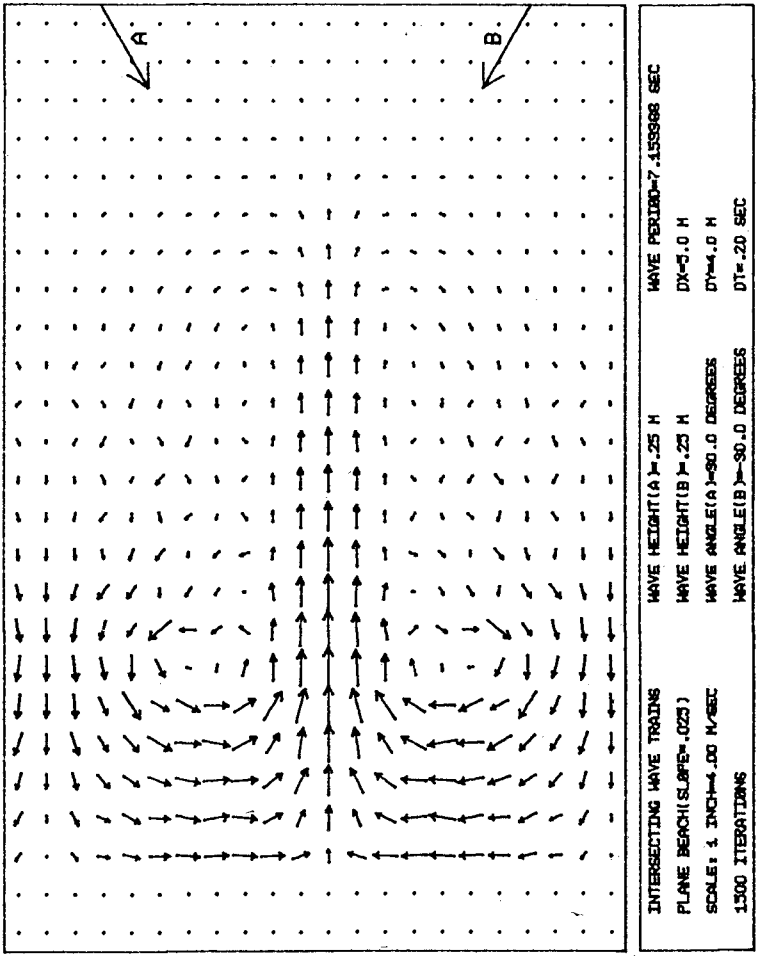

Figure 6. Current Vector Plot for a Rip Current Perpendicular to the Shoreline.

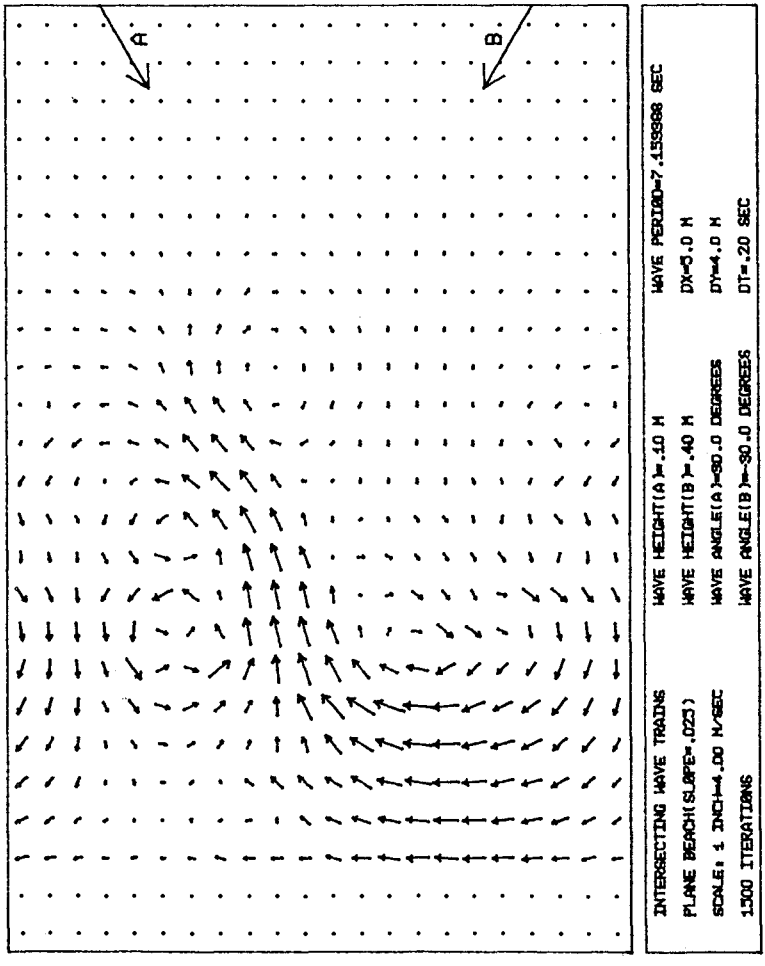

Figure 7, Current Vector Plot for the Meandering Circulation Pattern.

CONCLUSIONS

A model that can accurately predict currents and wave transformations in the nearshore zone is a necessary step in attempting to predict actual changes to our coastlines. From the results shown here it appears that the inclusion of the convective acceleration terms and lateral mixing terms in the horizontal momentum equations have important effects which must be included in models used to predict nearshore circulation. The terms become especially significant in attempts to model circulation over irregular bottom topographies which include bars and channels.

APPENDIX A - PERIODIC BOTTOM TOPOGRAPHY

The periodic bottom profile used in the model was developed by Noda et al. (14). The depths are given by

$$h = mx\left\{1 + A \exp\left[-3\left(\frac{x}{20}\right)^{1/3}\right]\sin^{10}\frac{\pi}{\lambda}(y - x\tan\beta)\right\}$$

where m = beach slope = .025.
x,y are the coordinates of the depth location.
λ = length of periodic beach = 80 meters.
A = amplitude of bottom variation = 20.
β = angle of rip channel to beach normal = 30 degrees.

The grid spacing was chosen to be 5.0 and 4.0 meters in the x and y directions, respectively. There were 25 and 21 grids in the x and y directions. The last grid row and the "dry" grid rows were made planar with the slope being .025.

REFERENCES

1. Allender, J. H., Ditmars, J. D., Harrison, W. and Paddock, R. A., "Comparison of Model and Observed Nearshore Circulation," Proceedings of the 16th International Conference on Coastal Engineering, Hamburg, 1978.

2. Birkemeier, W. A. and Dalrymple, R. A., "Nearshore Water Circulation Induced by Wind and Waves," Proceedings of the Symposium on Modeling Technique, ASCE, 1975, pp. 1062-1081. Also, "Numerical Models for the Prediction of Wave Set-Up and Nearshore Circulation", ONR Tech. Rept. No. 1 and Ocean Eng. Rept. No. 3, Dept. of Civil Eng., Univ. of Del., Jan. 1976.

3. Blumberg, A. F., "Numerical Tidal Model of Chesapeake Bay," Journal of the Hydraulics Division, ASCE, Vol. 103, No. HY1, January, 1977, pp. 1-9.

4. Dalrymple, R. A., "A Mechanism for Rip Current Generation on an Open Coast," Journal of Geophysical Research, Vol. 80, 1975, pp. 3485-3487.

5. Dalrymple, R. A., "Rip Currents and Their Genesis," Proceedings of the 16th International Conference on Coastal Engineering, Hamburg, 1978.

6. Holland, W. R. and Lin, L. B., "On the Generation of Mesoscale Eddies and Their Contribution to the Oceanic General Circulation. I. A Preliminary Numerical Experiment," Journal of Physical Oceanography, Vol. 5, October, 1975, pp. 642-657.

7. Kurihara, Y., "On the Use of Implicit and Iterative Methods for Time Integration of the Wave Equation," Monthly Weather Review, Vol. 93, No. 1, January, 1965, pp. 33-46.

8. Lilly, D. K., "On the Computational Stability of Numerical Solutions of Time-Dependent Non-Linear Geophysical Fluid Problems," Monthly Weather Review, Vol. 93, No. 1, January 1965.

9. Liu, P. L.-F. and Dalrymple, R. A., "Bottom Frictional Stresses and Longshore Currents Due to Waves with Large Angles of Incidence," Sears Foundation: Journal of Marine Research, Vol. 36, No. 2, May, 1978, pp. 357-375.

10. Liu, P. L.-F., and Lennon, G. P., "Finite Element Modeling of Nearshore Currents," Journal of the Waterway, Port, Coastal and Ocean Division, ASCE, Vol. 104, No. WW2, May, 1978, pp. 175-189.

11. Longuet-Higgins, M. S., "Longshore Currents Generated by Obliquely Incident Sea Waves, 1," Journal of Geophysical Research, Vol. 75, No. 33, November, 1970, pp. 6778-6789.

12. Longuet-Higgins, M. S., "Longshore Currents Generated by Obliquely Incident Sea Waves, 2," Journal of Geophysical Research, Vol. 75, No. 33, November, 1970, pp. 6790-6801.

13. Longuet-Higgins, M. S. and Stewart, R. W., "Radiation Stress and Mass Transport in Gravity Waves with Application to Surf Beat," Journal of Fluid Mechanics, Vol. 13, 1962, pp. 481-504.

14. Noda, E. K., Sonu, C. J., Rupert, V. C. and Collins, J. I., "Nearshore Circulations Under Sea Breeze Conditions and Wave-Current Interactions in the Surf Zone," Tetra Tech Report TC-149-4, February, 1974.

15. Phillips, O. M., The Dynamics of the Upper Ocean, Cambridge University Press, 1969, pp. 45-48.

ACKNOWLEDGEMENTS

This study was supported by the Office of Naval Research, Geography Programs, Arlington, VA. Alan F. Blumberg was very helpful in the early stages of this study.